Bonding Analysis

International Edition: DOI: 10.1002/anie.201503686
German Edition: DOI: 10.1002/ange.201503686

Formation and Characterization of the Boron Dicarbonyl Complex $[B(CO)_2]^-$

Qingnan Zhang, Wan-Lu Li, Cong-Qiao Xu, Mohua Chen, Mingfei Zhou, Jun Li,* Diego M. Andrada, and Gernot Frenking**

Dedicated to Professor Peter Paetzold on the occasion of his 80th birthday

Abstract: *We report the synthesis and spectroscopic characterization of the boron dicarbonyl complex $[B(CO)_2]^-$. The bonding situation is analyzed and compared with the aluminum homologue $[Al(CO)_2]^-$ using state-of-the-art quantum chemical methods.*

In 1906, Diels and Wolf reported the synthesis of the compound C_3O_2 which they named carbon suboxide ("Kohlensuboxyd").[1] They described the bonding situation with the symbols OC:C:CO, which was the prevailing notation at that time. The symbols changed in the course of time to OC=C=CO that indicate conventional carbon–carbon double bonds like in allene $H_2C{=}C{=}CH_2$. However, already in 1953 the infrared fine structure of C_3O_2 casted some doubt on the linear structure of the molecule.[2] A definite answer was given by P. Jensen in 1986 through investigation of the experimental vibrational spectrum which revealed a bending angle of 156° at the central carbon atom.[3] This result is in excellent agreement with the ab initio value of 155.9° calculated at the CCSD(T)/cc-pVQZ level by Koput.[4] The bending potential of C_3O_2 is very flat (< 0.5 kcal mol^{-1}),[3,4] which explains why the molecule becomes linear in the solid state.[5]

The nonlinear structure of C_3O_2 has been explained in terms of dative bonds between two carbonyl ligands and the carbon atom in its excited ^{1}D state OC→C←CO, which has the electron configuration $2s^2,2p(\sigma)^0,2p(\pi_\parallel)^0,2p(\pi_\perp)^2$ in the molecule.[6] Thus, C_3O_2 should better be classified as a carbonyl complex of carbon $[C(CO)_2]$ rather than a carbon oxide such as CO or CO_2.[7] The different bonding situation compared with linear allene $H_2C{=}C{=}CH_2$, which has a deep potential well, can be rationalized with the $^3B_1$ triplet ground state of CH_2, which preferentially engages in normal covalent ("electron-sharing") bonds A–B. In contrast, CO has a singlet ground state with the lowest lying $a^3\Pi$ triplet state being 139.2 kcal mol^{-1} higher in energy.[8] Therefore, CO binds preferentially through donor–acceptor interactions A→B.[9]

The bonding model of donor–acceptor interactions straightforwardly explains the strongly bent equilibrium geometry of isoelectronic $[N(CO)_2]^+$, which has an experimental ∡C-N-C angle of 130.7°.[10] The contribution of π-backdonation OC←N^+→CO to the carbonyl bonding is much weaker than that in carbon suboxide OC←C→CO. A reverse trend may be expected from the negatively charged boron complex $[B(CO)_2]^-$, in which strong π-backdonation OC←B^-→CO should yield a larger bond angle than in $C(CO)_2$. In this paper we report the isolation of linear $[B(CO)_2]^-$ in a low-temperature matrix and its identification by the experimental and calculated vibrational spectra. We also present a thorough theoretical analysis of the bonding of the anion and compare it with the structure of the aluminum homologue $[Al(CO)_2]^-$, which has a strongly bent equilibrium geometry.[11] To the best of our knowledge, $[B(CO)_2]^-$ is the first experimentally observed carbonyl of charged boron atom.

The boron carbonyl species are prepared by co-condensation of the reactive species generated by laser ablation of bulk boron target with CO/Ne mixtures onto a CsI window at 4 K as previously described.[12] The product species are characterized by infrared absorption spectroscopy employing a Bruker Vertex 80 V spectrometer at 0.5 cm^{-1} resolution using a liquid-nitrogen cooled mercury cadmium telluride (MCT) detector. Natural abundance boron (^{10}B, 19.8%; ^{11}B, 80.2%) and ^{10}B-enriched (97%) targets are used in different experiments. Isotope-substituted CO samples ($^{13}C^{16}O$, $^{12}C^{18}O$, $^{12}C^{16}O + {}^{13}C^{16}O$, and $^{12}C^{16}O + {}^{12}C^{18}O$) are also employed for product identification based on isotopic shifts and band splitting. Anions usually have small ionization energies, thus electrons can be easily detached from them by visible or ultraviolet irradiation. As laser ablation of the bulk boron target produces a plume of radiation, and the samples were

[*] Q. Zhang, Dr. M. Chen, Prof. M. Zhou
Collaborative Innovation Center of Chemistry for Energy Materials
Department of Chemistry, Shanghai Key Laboratory of Molecular Catalysts and Innovative Materials, Fudan University
Shanghai 200433 (China)
E-mail: mfzhou@fudan.edu.cn
W.-L. Li, C.-Q. Xu, Prof. J. Li
Department of Chemistry & Key Laboratory of Organic Optoelectronics and Molecular Engineering of Ministry of Education
Tsinghua University
Beijing 100084 (China)
E-mail: junli@tsinghua.edu.cn
Dr. D. M. Andrada, Prof. G. Frenking
Fachbereich Chemie, Philipps-Universität Marburg
Hans-Meerwein-Strasse, 35043 Marburg (Germany)
E-mail: frenking@chemie.uni-marburg.de
Prof. G. Frenking
Donostia International Physics Center (DIPC)
P.K. 1072, 20080 Donostia (Spain)

Supporting information for this article is available on the WWW under http://dx.doi.org/10.1002/anie.201503686.

deposited with concurrent irradiation, the photosensitive anion species cannot survive using high laser energy. Thus, the experiments are performed employing relatively low laser energy to minimize the plume of irradiation and to favor the trapping of anion species in solid neon.[13a]

The infrared spectra in the C–O and B–C stretching frequency regions using a ^{10}B-enriched target and 0.025 % CO are shown in Figure 1. Strong carbonyl stretching vibrations from the boron carbonyl neutral species are observed. The

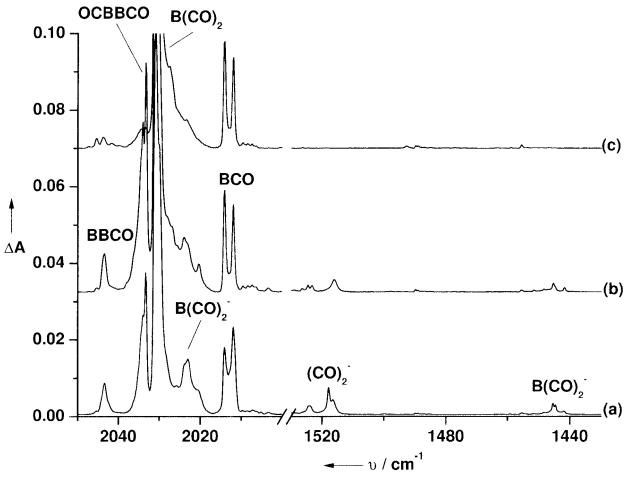

Figure 1. Infrared spectra in the 2050–2000 and 1530–1430 cm^{-1} regions from co-deposition of ^{10}B-enriched (97 %) boron atoms with 0.025 % CO in solid neon. a) after 30 min of sample deposition at 4 K, b) after 12 K annealing, and c) after 15 min of UV-visible ($280 < \lambda < 580$ nm) irradiation.

split bands at 2014.2/2012.0 and 1150.9/1149.2 cm^{-1} are attributed to the C–O and B–C stretching vibrations of the ^{10}BCO molecule at two trapping sites. The same modes were previously observed at 2007.3 and 1148.1 cm^{-1} in solid argon,[13b,14] which characterized a $^4\Sigma$ electronic ground state of the molecule.[15] The 2043.5 cm^{-1} band corresponds to the band reported at 2031.9 cm^{-1} that was previously assigned to the C–O stretching vibration of the $^{10}B^{10}BCO$ molecule, a σ–π diradical.[16] The bands at 2033.3, 1116.3, and 523.1 cm^{-1} are assigned to the $OC^{10}B^{10}BCO$ molecule in solid neon, which was characterized to be a boron–boron triple-bonded species.[17] The corresponding modes in solid argon are observed at 2016.4, 1116.5, and 521.4 cm^{-1}.[17a] The strongest band at 2031.1 cm^{-1} can be attributed to the antisymmetric C–O stretching vibration of the linear $^{10}B(CO)_2$ molecule in solid neon (2022.5 cm^{-1} in solid argon).[15]

Besides the above-mentioned neutral boron carbonyl absorptions, photosensitive bands at 2024.2, 1517.8/1516.1, and 1445.4 cm^{-1} are also observed on sample deposition. The 1517.8/1516.1 cm^{-1} bands are due to the $(CO)_2^-$ anion that are common to other laser-ablated metal reactions with CO in solid neon.[18] The bands at 2024.2 and 1445.4 cm^{-1} are observed only in the present neon matrix experiments using low laser energy. Both bands are observed after sample deposition and remain almost unchanged upon sample annealing, but both are destroyed when the sample is subjected to UV light irradiation ($280 < \lambda < 400$ nm) and their intensity cannot be recovered on subsequent sample annealing to high temperatures. Along with the elimination of the 2024.2 and 1445.4 cm^{-1} bands, the neutral $B(CO)_2$ absorption band increases in concert. The upper band shows very similar B/C/O isotopic shifts as those of the neutral $B(CO)_2$ molecule. The band position and isotopic shifts indicate that it is a carbonyl stretching vibration. The much weaker 1445.4 cm^{-1} band can be attributed to a B–C stretching vibration. The spectra in the 1455–1400 cm^{-1} region using different isotope-labeled samples are shown in Figure 2. The spectra clearly demonstrate that the new

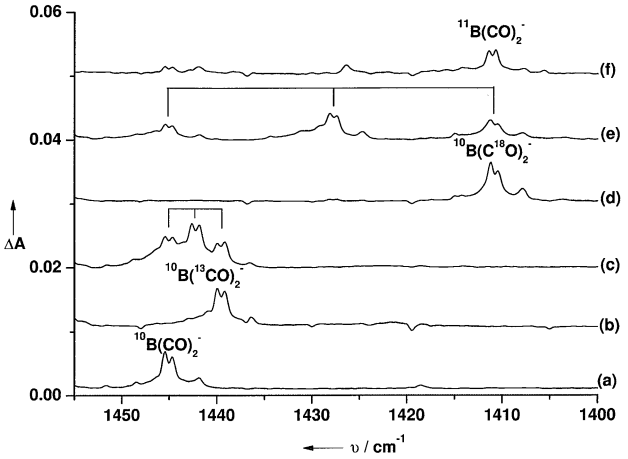

Figure 2. Infrared spectra in the 1455–1400 cm^{-1} region from co-deposition of laser-ablated boron atoms with isotope-labeled CO in excess neon. Spectra were taken after 30 min of sample deposition at 4 K. a) $^{10}B + 0.025\,\%\ ^{12}C^{16}O$, b) $^{10}B + 0.025\,\%\ ^{13}C^{16}O$, c) $^{10}B + 0.025\,\%\ ^{12}C^{16}O + 0.025\,\%\ ^{13}C^{16}O$, d) $^{10}B + 0.025\,\%\ ^{12}C^{18}O$, e) $^{10}B + 0.02\,\%\ ^{12}C^{16}O + 0.02\,\%\ ^{12}C^{18}O$, and f) natural abundance boron (19.8 % $^{10}B + 80.2\,\%\ ^{11}B$) + 0.025 % $^{12}C^{16}O$.

product species involves only one B and two equivalent CO subunits, and can thus be assigned to a species with a $B(CO)_2$ formula. The photosensitive behavior implies that this species is most likely due to a charged species. To verify the charge state of this species, an additional experiment is performed by adding CCl_4 to serve as an electron trap.[19] The 2024.2 and 1445.4 cm^{-1} bands as well as the $(CO)_2^-$ absorption are almost absent from the spectrum with 0.01 % CCl_4 added to the neon matrix gas. These results indicate that the new absorptions can confidently be assigned to the $[B(CO)_2]^-$ anion species. The observation of only one C–O stretching and one B–C stretching vibration implies that the $[B(CO)_2]^-$ anion is linear.

To verify the assignments of the experimentally observed vibrational modes, we performed ab initio calculations at the CCSD(T)/aug-cc-pVTZ level of theory[20] of $[B(CO)_2]^-$ for various atomic isotopes. Figure 3 shows the optimized geometries of CO, $[ACO]^-$, and $[A(CO)_2]^-$ (A = B, Al). The boron anion $[B(CO)_2]^-$ exhibits a linear equilibrium structure, as expected from the IR spectra. The calculated C–O distance (1.200 Å) is longer than in neutral CO (1.136 Å), which agrees with the observed redshift of the C–O stretching mode of the anion.[21] The calculated vibrational frequencies for the

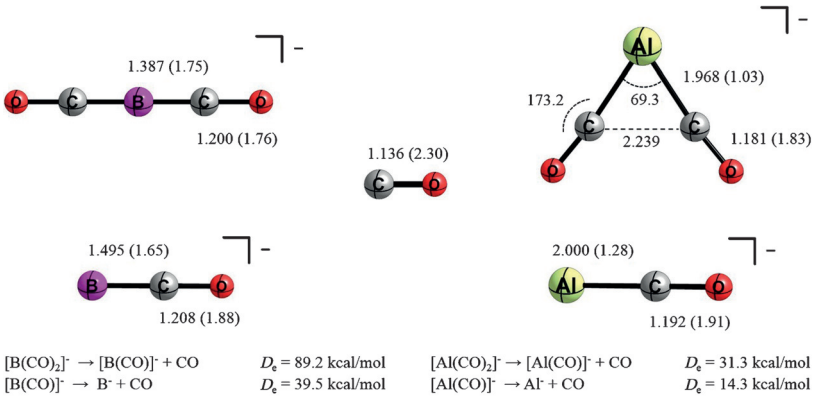

Figure 3. Optimized geometries of CO, $[B(CO)_2]^-$, and $[Al(CO)_2]^-$ at the CCSD(T)/aug-cc-pVTZ level. Bond lengths are given in [Å] and angles in [°]. The values in parentheses give the Wiberg bond orders. Calculated dissociation energies (D_e) for loss of CO are given in kcal mol^{-1}.

antisymmetric C–O and B–C stretching modes are given in Table 1. The theoretical values are slightly higher than the experimental data due to the harmonic approximation.[22] There is excellent agreement between the experimental and calculated frequency shifts for all isotopes in both stretching modes, which leaves no doubt that the assignment of the vibrational frequencies to the boron dicarbonyl anion $[B(CO)_2]^-$ is correct.

Table 1: Infrared absorptions of $[B(CO)_2]^-$ and $[Al(CO)_2]^-$. Experimental (calculated at CCSD(T)/aug-cc-pVTZ) vibrational frequencies of the antisymmetric C–O and B–C stretching modes. Frequency shifts for isotope exchange $\Delta\nu$. All data in cm^{-1}.

Molecule	Mode	$^{12}C^{16}O$	$^{13}C^{16}O$	$^{12}C^{18}O$
$^{10}B(CO)_2^-$	asym. CO str.	2024.0 (2068)	1979.8 (2025)	–[a] (2058)
	$\Delta\nu$ $^{12}C^{16}O$ →	–	44.2 (43.0)	–[a] (10)
	asym. BC str.	1445.4 (1455)	1440.0 (1450)	1411.2 (1420)
	$\Delta\nu$ $^{12}C^{16}O$ →	–	5.4 (5)	34.2 (35)
$^{11}B(CO)_2^-$	asym. CO str.	1992.7 (2035)	1951.6 (1990)	1976.0 (2023)
	$\Delta\nu$ $^{12}C^{16}O$ →	–	41.1 (45)	16.7 (12)
	$\Delta\nu$ ^{10}B → ^{11}B	31.3 (33)	28.2 (35)	–[a] (35)
	asym. BC str.	1411.4 (1421)	1407.6 (1417)	1378.9 (1387)
	$\Delta\nu$ $^{12}C^{16}O$ →	–	3.8 (4)	32.5 (34)
	$\Delta\nu$ ^{10}B → ^{11}B	34.0 (34)	32.4 (33)	32.3 (33)
$Al(CO)_2^-$	sym. CO str.	1812.0 (1828)	1770.5 (1788)	1770.4 (1786)
	$\Delta\nu$ $^{12}C^{16}O$ →	–	41.5 (40)	41.6 (42)
	asym. CO str.	1750.8 (1771)	1710.8 (1730)	1711.9 (1730)
	$\Delta\nu$ $^{12}C^{16}O$ →	–	40.0 (41)	38.9 (41)

[a] Masked by the strong boron carbonyl neutral absorptions.

The $[B(CO)_2]^-$ anion is formed by electron capture of the neutral $[B(CO)_2]$ molecule during sample deposition. The adiabatic electron affinity of $[B(CO)_2]$ is predicted to be 58.1 kcal mol^{-1}. The calculated electron vertical detachment energy of $[B(CO)_2]^-$ (57.4 kcal mol^{-1}) is smaller than the bond dissociation energies for loss of one CO from $[B(CO)_2]^-$ (D_e = 89.2 kcal mol^{-1}) and $B(CO)_2$ (D_e = 61.1 kcal mol^{-1}), which is consistent with the experimental observation that $[B(CO)_2]^-$ is photobleached to form neutral $[B(CO)_2]$ under UV-visible light irradiation.

In contrast to the boron dicarbonyl anion, the calculated equilibrium geometry of the aluminum homologue $[Al(CO)_2]^-$ has a very acute bending angle C-Al-C of 69.3°. Both the symmetric and antisymmetric C–O stretching vibrations of the bent $[Al(CO)_2]^-$ anion are IR active, which were observed at 1803.9 and 1741.0 cm^{-1} in solid argon.[11] The neon matrix experiments give slightly blue-shifted values of 1812.0 and 1750.8 cm^{-1} (Figures S1 and S2 in the Supporting Information). The calculated frequency shifts for isotope exchange on the C–O vibrations of $[Al(CO)_2]^-$ concur with the experimental data (Table 1). The calculated C–O distance in the boron complex (1.200 Å) is longer than that of $[Al(CO)_2]^-$ (1.181 Å). This is in accord with the results of the bonding analysis discussed below which shows that the $[B(CO)_2]^-$ anion has two doubly occupied orbitals involving B^- to CO π-backdonation interaction, whereas the $[Al(CO)_2]^-$ anion has only one. We are also to point out that there is a small inwards-bending of the Al-C-O moiety with a bending angle of 173.2°. However, the C–C distance of 2.239 Å in the aluminum complex is too long to suggest direct carbon–carbon bonding. The bent equilibrium structure of $[Al(CO)_2]^-$ is calculated at the CCSD(T)/aug-cc-pVTZ level to be 42.1 kcal mol^{-1} lower in energy than the linear form. In contrast, the bending potential of $[B(CO)_2]^-$ is very shallow. The energy difference between the linear equilibrium structure and a geometry with a fixed bending angle of 130° is only 1.1 kcal mol^{-1}. The theoretically predicted BDEs suggest that also for the aluminum complex the second CO is more strongly bonded (D_e = 31.3 kcal mol^{-1}) than the first CO (D_e = 14.3 kcal mol^{-1}).

We analyzed the electronic structures of $[B(CO)_2]^-$ and $[Al(CO)_2]^-$ to understand the different geometries and bonding situations. The first question that we address concerns the nature of the boron–CO interactions in linear $[B(CO)_2]^-$, which can be described with a classical Lewis structure $OC{=}B^{(-)}{=}CO$ or with dative bonds $OC{\rightleftarrows}B^{(-)}{\rightleftarrows}CO$ following the Dewar–Chatt–Duncanson (DCD) model.[23] We are using the sign for a double arrow ⇄ to emphasize that there is not only σ-donation $OC{\rightarrow}B^{(-)}{\leftarrow}CO$ but also degenerate π-backdonation $OC{\leftarrow}B^{(-)}{\rightarrow}CO$ which can be expected to be rather strong due to the negatively charged boron atom. This description would generate a significant multiple-bond character as it was previously shown for $OC{\rightleftarrows}BB{\rightleftarrows}CO$.[17] The two types of bonding actually arise from different types of covalent interactions and thus, the different formulas are not a mere

Table 2: Energy decomposition analysis of $[B(CO)_2]^-$ and $[Al(CO)_2]^-$ at the BP86/TZ2P+ level. Energy values are given in kcal mol^{-1}.

Fragments	B^- $2s^0 2p(\sigma)^0 2p(\pi)^2 2p(\pi')^2$ (OC)···(CO) Singlet state	B^- $2s^1 2p(\sigma)^1 2p(\pi)^1 2p(\pi')^1$ (OC)···(CO) Quintet state	Al^- $3s^2,3p(\sigma)^0,3p(\pi_\parallel)^0,3p(\pi_\perp)^2$ (OC)···(CO) Singlet state
ΔE_{int}	−445.3	−488.0	−98.6
ΔE_{Pauli}	116.7	335.0	218.9
ΔE_{elstat} [a]	−128.6 (22.9%)	−329.2 (40.0%)	−124.7 (39.3%)
ΔE_{orb} [a]	−433.4 (77.1%)	−493.9 (60.0%)	−192.7 (60.7%)
ΔE_1 [b] OC←E$^{(-)}$→CO	−127.7 (29.5%)	−87.3 (17.7%)	−99.2 (51.5%)
ΔE_2 [b] OC←E$^{(-)}$→CO	−127.7 (29.5%)	−87.3 (17.7%)	−54.7 (28.4%)
ΔE_3 [b] σ(+,−) OC→E$^{(-)}$←CO	−114.2 (26.3%)	−151.7 (30.7%)	−19.5 (10.1%)
ΔE_4 [b] σ(+,+) OC→E$^{(-)}$←CO	−54.8 (12.6%)	−151.0 (30.6%)	−15.7 (8.1%)
ΔE_{orb}(rest) [b]	−8.6 (2.0%)	−16.9 (3.4%)	−3.6 (1.9%)

[a] The value in parentheses gives the percentage contribution to the total attractive interactions $\Delta E_{elstat} + \Delta E_{orb}$. [b] The value in parentheses gives the percentage contribution to the total orbital interactions ΔE_{orb}.

formality but they indicate dissimilar chemical bonding.[24] How can they be distinguished?

To answer this question we carried out EDA-NOCV (energy decomposition analysis with natural orbitals for chemical valency)[25] calculations of $[B(CO)_2]^-$ using two different fragmentation schemes which are suggested by normal covalent (electron-sharing) bonding OC=B$^{(-)}$=CO and by donor–acceptor interactions OC⇄B$^{(-)}$⇄CO. The associated fragments for electron-sharing interactions are B$^{(-)}$ in the ^{5}S state with four unpaired electrons and $(CO)_2$ in the associated quintet state. The symmetry-adapted fragments for the donor–acceptor interactions are $(CO)_2$ in the electronic singlet state and B$^{(-)}$ with the associated valence electron configuration $2s^0,2p(\sigma)^0,2p(\pi)^2,2p(\pi')^2$. The first two vacant valence AOs are then available for σ-donation OC→B$^{(-)}$←CO, whereas the occupied 2p(π) AOs donate electronic charge for the π-backdonation OC←B$^{(-)}$→CO. Table 2 shows the calculated numerical results.

The crucial data indicating the best choice for the interacting fragments come from the orbital term. Those EDA-NOCV calculations that give the smallest ΔE_{orb} value indicate which fragments are the best choice for describing the bonding situation, because the least alteration of the electronic charge distribution is required to yield the electronic structure of the molecule.[26] Table 2 shows that the choice of the singlet fragments give a clearly smaller absolute value of $\Delta E_{orb} = -433.4$ kcal mol^{-1} than the quintet fragments with $\Delta E_{orb} = -493.9$ kcal mol^{-1}. The breakdown of the orbital term into pairwise contributions gives four major terms ΔE_1–ΔE_4 which can easily be identified by visual inspection of the associated deformation densities $\Delta\rho_1$–$\Delta\rho_4$, as shown in Figure 4 a–d. The color code of the deformation densities indicates the direction of the charge flow red→blue. The principle orbital interactions which are connected to the deformation densities are schematically shown in Figure 4 e. It becomes apparent that the strongest degenerate contributions ΔE_1 and ΔE_2 (−127.7 kcal mol^{-1} each) come from the π-backdonation OC←B$^{(-)}$→CO. The slightly weaker stabilization $\Delta E_3 = -114.2$ kcal mol^{-1} arises from the out-of-phase (+,−) σ-donation of the CO lone pair orbitals OC→B$^{(-)}$←CO into the vacant p(σ) AO of boron. It is interesting to note that the in-phase (+,+) σ-donation OC→B$^{(-)}$←CO into the vacant 2s AO of boron is much weaker ($\Delta E_4 = -54.8$ kcal mol^{-1}) than the out-of-phase (+,−) σ-donation,

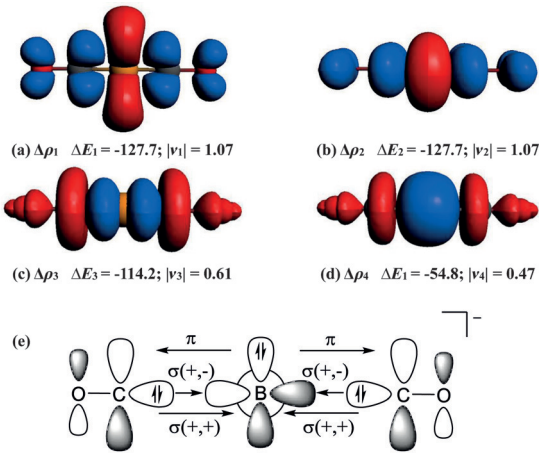

Figure 4. a–d) Plot of deformation densities $\Delta\rho_1$–$\Delta\rho_4$ (isocontour 0.003 a.u.) of the pairwise orbital interactions in $[B(CO)_2]^-$ together with the associated interaction energies ΔE_n and charge eigenvalues $|\nu_n|$ (in e). The charge flow is red→blue. The charge eigenvalues ν give the amount of donated/accepted electronic charge. e) Schematic representation of the orbitals involved in the OC→B$^{(-)}$←CO σ-donation and the OC←B$^{(-)}$→CO π-backdonation. Only one component of the latter is shown.

although the 2s AO is energetically lower lying than the 2p AO. The stronger stabilization of the donation into the latter comes from the larger overlap of the p(σ) AO than the 2s AO of boron with the donor orbitals. We emphasize that the eigenvalues of the deformation densities $|\nu_n|$ (in Figure 4) which indicate the amounts of charge transfer are not directly related to the strength of the stabilization energy. Examples for carbonyl complexes in which π-backdonation is stronger than σ-donation have previously been reported for transition metal complexes.[27]

Table 2 also gives the results of the EDA-NOCV calculations of $[Al(CO)_2]^-$ using the singlet fragments (OC)···(CO) and Al^- with the valence electron configuration $3s^2,3p(\sigma)^0,3p(\pi_\parallel)^0,3p(\pi_\perp)^2$. We draw attention to the difference between the occupation of the valence AOs of Al^- and B^-, which is associated with the bent versus linear geometries of the dicarbonyl complexes. The donor–acceptor interactions of the boron complex are very strong, which compensate for the $2s^2 \rightarrow 2p^2$ excitation energy required to achieve the electronic

reference of B^-. The much weaker carbonyl bonding in $[Al(CO)_2]^-$ is not large enough to pay for the excitation $3s^2 \rightarrow 3p^2$, which explains why the boron species is linear whereas aluminum is bent.

The orbital interactions ΔE_{orb} in $[Al(CO)_2]^-$ have four major contributions like in the boron homologue $\Delta E_1 - \Delta E_4$. Inspection of the associated deformation densities $\Delta\rho_1 - \Delta\rho_4$, as displayed in Figure 5 a–d, gives detailed insight into the nature of the donor–acceptor interactions in the complex.

Like in the boron homologue the strongest contribution $\Delta E_1 = -99.2$ kcal mol^{-1} in $[Al(CO)_2]^-$ comes from π-backdonation OC←Al$^{(-)}$→CO. Note that the deformation density ρ_1 suggests some charge accumulation between the carbon atoms (blue region). The much weaker energy terms $\Delta E_3 = -19.5$ kcal mol^{-1} and $\Delta E_4 = -15.7$ kcal mol^{-1} are easily identified with the (+,−) and (+,+) σ-donation of the CO lone pair orbitals OC→Al$^{(-)}$←CO. The most interesting information comes from the deformation density $\Delta\rho_2$, which is connected to the second strongest orbital term $\Delta E_2 = -54.7$ kcal mol^{-1}. There is an area of both red and blue deformation density at Al, which indicates strong polarization (hybridization) at aluminum. The hybridization comes from mixing the 3s and 3p(σ) AO of Al$^{(-)}$ and is caused by the interactions with the CO ligands. Figure 5 e schematically shows the 3s/3p(σ) hybridization that affects the orbital interactions related to the stabilization energies ΔE_2 and ΔE_4. The occupied $3s^2$ and the vacant $3p(\sigma)^0$ AO give a vacant $3sp^0$-hybridized orbital that serves as acceptor orbital in the (+,+) σ-donation OC→Al$^{(-)}$←CO. The corresponding occupied 3sp orbital becomes a donor orbital for OC←Al$^{(-)}$→CO back-donation into the in-plane π* orbitals of (OC)···(CO). Note that the symmetry assignment π* refers to isolated CO whereas the interacting orbitals have σ symmetry with respect to the molecular plane. The acceptor orbital of (OC)···(CO) in the orbital term ΔE_2 has σ symmetry. The rather large stabilization energy $\Delta E_2 = -54.7$ kcal mol^{-1} comes partly from the polarization of the electronic charge at the atoms.

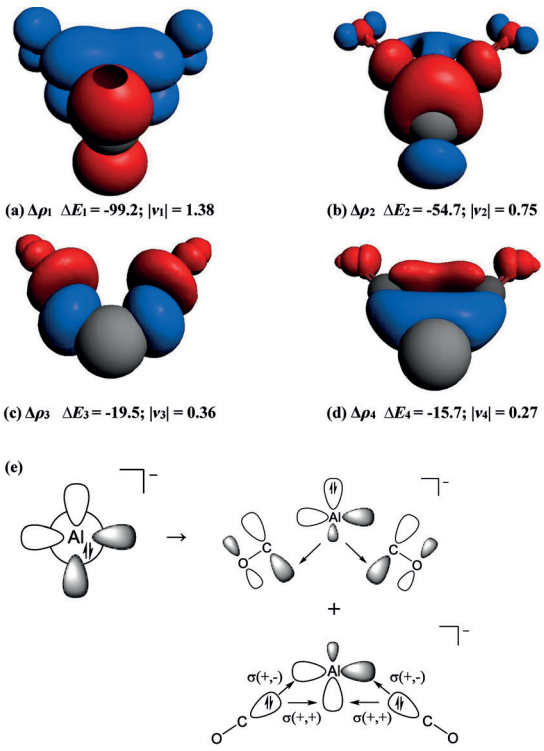

Figure 5. a–d) Plot of deformation densities $\Delta\rho_1 - \Delta\rho_4$ (isocontour 0.003 a.u.) of the pairwise orbital interactions in $[Al(CO)_2]^-$ together with the associated interaction energies ΔE_n and charge eigenvalues $|\nu_n|$ (in e). The charge flow is red→blue. The charge eigenvalues ν give the amount of donated/accepted electronic charge. e) Schematic representation of the polarization of the 3s and 3p(σ) AOs of Al$^{(-)}$ and the donor–acceptor interactions associated with $\Delta\rho_2$ and $\Delta\rho_4$. Note that the π orbitals are not shown.

The EDA-NOCV results can nicely be connected to conventional information of the electronic structures. For example, the occupied valence orbitals of $[B(CO)_2]^-$ and $[Al(CO)_2]^-$ (Figures S3 and S4) mirror the charge flow indicated by the deformation densities $\Delta\rho_1 - \Delta\rho_4$. The degenerate π HOMO of $[B(CO)_2]^-$ reflects the π-backdonation OC←B$^{(-)}$→CO whereas the HOMO-3 and HOMO-4 are connected to the (+,−) and (+,+) σ-donation OC→B$^{(-)}$←CO, respectively. Similarly, the HOMO of $[Al(CO)_2]^-$ is related to the OC←Al$^{(-)}$→CO π-backdonation whereas the HOMO-1 is connected to the OC←Al$^{(-)}$→CO σ-backdonation. However, the MOs do not give information about the strength of the interactions and the pairwise charge donation sometimes involves more than one fragment MO. Thus, although the (+,−) σ-donation OC→Al$^{(-)}$←CO, is connected to the HOMO-2, the (+,+) σ-donation involves the mixing of HOMO-7 and HOMO-9. Note that the deformation densities $\Delta\rho_1$ and $\Delta\rho_2$ of $[Al(CO)_2]^-$ reveal some charge flow into the carbon–carbon bonding region, which signals attractive interactions that explain the acute bonding angle and the slight inward bending of the Al-C-O moieties. Figure S5 shows that there is indeed a carbon–carbon bond path in the complex which, however, does not indicate a genuine chemical bond.[28]

In summary, this work reports the synthesis and spectroscopic characterization of the boron dicarbonyl complex $[B(CO)_2]^-$. A detailed analysis of the electronic structure using state-of-the-art methods suggests that the bonding situation is best described in terms of donor–acceptor interactions OC⇄B$^{(-)}$⇄CO between B$^{(-)}$ with the valence electron configuration $2s^0,2p(\sigma)^0,2p(\pi)^2,2p(\pi')^2$ and the CO ligands in which the π-backdonation OC←B$^{(-)}$→CO is stronger than the σ-donation OC→B$^{(-)}$←CO.

After finishing this work, we learned that the associated neutral boron dicarbonyl complex [(RB)(CO)$_2$] in which R is a bulky aryl group has been synthesized and structurally characterized by X-ray crystallography by Braunschweig and co-workers.[29] The chemical behavior shows typical features of carbonyl complexes which are known from transition metal carbonyls. This is further support for the suggestion that the anion $[B(CO)_2]^-$ is a boron complex.

Acknowledgements

The work at Fudan was financially supported by the National Natural Science Foundation (Grant Nos. 21173053 and

21433005), the Ministry of Science and Technology of China (2013CB834603), and the Committee of Science and Technology of Shanghai (13XD1400800). J.L. acknowledges financial support by the NSFC (Grant Nos. 21221062 and 91426302). The work at Marburg was supported by the Deutsche Forschungsgemeinschaft (FR 641/25-1). D.M.A. thanks the Deutscher Akademischer Austauschdienst for a postdoctoral fellowship. Part of the calculations was performed at the Tsinghua National Laboratory for Information Science.

Keywords: bonding analysis · boron dicarbonyl compound · matrix isolation · quantum chemical calculations

How to cite: *Angew. Chem. Int. Ed.* **2015**, *54*, 11078–11083
Angew. Chem. **2015**, *127*, 11230–11235

[1] O. Diels, B. Wolf, *Ber. Dtsch. Chem. Ges.* **1906**, *39*, 689.
[2] D. Rix, *J. Chem. Phys.* **1953**, *22*, 429.
[3] P. Jensen, J. W. C. Johns, *J. Mol. Spectrosc.* **1986**, *118*, 248.
[4] J. Koput, *Chem. Phys. Lett.* **2000**, *320*, 237.
[5] A. Ellern, T. Drews, K. Seppelt, *Z. Anorg. Allg. Chem.* **2001**, *627*, 73.
[6] a) M. A. Celik, R. Sure, S. Klein, R. Kinjo, G. Bertrand, G. Frenking, *Chem. Eur. J.* **2012**, *18*, 5676.
[7] It is interesting to note that Diels and Wolf wrote in their original paper that C_3O_2 noticeably reminds of metal carbonyls. They point out that carbon is capable like metals to add CO yielding volatile and highly reactive carbonyls.[1]
[8] a) R. W. Field, S. G. Tilford, R. A. Howard, J. D. Simmons, *J. Mol. Spectrosc.* **1972**, *44*, 347; b) C. T. Falzon, D. P. Chong, F. Wang, *J. Comput. Chem.* **2006**, *27*, 163.
[9] The high singlet–triplet gap of CO explains why until now there are only stable carbonyl complexes of transition metals [TM]→CO known but no metallaketenes [TM]=C=O.
[10] I. Bernhardi, T. Drews, K. Seppelt, *Angew. Chem. Int. Ed.* **1999**, *38*, 2232; *Angew. Chem.* **1999**, *111*, 2370.
[11] L. N. Zhang, J. Dong, M. F. Zhou, Q. Z. Qin, *J. Chem. Phys.* **2000**, *113*, 10169.
[12] G. J. Wang, M. F. Zhou, *Int. Rev. Phys. Chem.* **2008**, *27*, 1.
[13] a) M. F. Zhou, L. Andrews, C. W. Bauschlicher, Jr., *Chem. Rev.* **2001**, *101*, 1931; b) T. R. Burkholder, L. Andrews, *J. Phys. Chem.* **1992**, *96*, 10195.
[14] M. F. Zhou, N. Tsumori, L. Andrews, Q. Xu, *J. Phys. Chem. A* **2003**, *107*, 2458.
[15] a) Y. M. Hamrick, R. J. Van Zee, J. T. Godbout, W. Weltner, W. J. Lauderdale, J. F. Stanton, R. J. Bartlett, *J. Phys. Chem.* **1991**, *95*, 2840; b) A. J. Bridgeman, *J. Chem. Soc. Dalton Trans.* **1997**, 1323; c) A. Skancke, J. F. Liebman, *J. Phys. Chem.* **1994**, *98*, 13215.
[16] M. F. Zhou, Z. X. Wang, P. V. Schleyer, Q. Xu, *ChemPhysChem* **2003**, *4*, 763.
[17] a) M. F. Zhou, N. Tsumori, Z. H. Li, K. N. Fan, L. Andrews, Q. Xu, *J. Am. Chem. Soc.* **2002**, *124*, 12936; b) L. C. Ducati, N. Takagi, G. Frenking, *J. Phys. Chem. A* **2009**, *113*, 11693.
[18] a) W. E. Thompson, M. E. Jacox, *J. Chem. Phys.* **1991**, *95*, 735; b) M. F. Zhou, L. Andrews, *J. Am. Chem. Soc.* **1999**, *121*, 9171; c) M. F. Zhou, L. Andrews, J. Li, B. E. Bursten, *J. Am. Chem. Soc.* **1999**, *121*, 9712.
[19] M. F. Zhou, L. Andrews, *J. Am. Chem. Soc.* **1998**, *120*, 11499.
[20] For theoretical details see the Supporting Information.
[21] K. P. Huber, G. Herzberg, *Constants of Diatomic Molecules*, Van Nostrand-Reinhold, New York, **1979**.
[22] W. J. Hehre, L. Radom, P. v. R. Schleyer, J. A. Pople, *Ab Initio Molecular Orbital Theory*, Wiley, New York, **1986**.
[23] a) M. J. S. Dewar, *Bull. Soc. Chim. Fr.* **1951**, *18*, C79; b) J. Chatt, L. A. Duncanson, *J. Chem. Soc.* **1953**, 2929; c) G. Frenking, *J. Organomet. Chem.* **2001**, *635*, 9; d) G. Frenking, *Modern Coordination Chemistry: The Legacy of Joseph Chatt* (Eds.: G. J. Leigh, N. Winterton), The Royal Society, London, **2002**, p. 111.
[24] a) For a striking example of the different bonding situations of electron-sharing and dative bonds in related molecules see: K. C. Mondal, H. W. Roesky, M. C. Schwarzer, G. Frenking, S. Neudeck, I. Tkach, H. Wolf, D. Kratzert, R. Herbst-Irmer, B. Niepötter, D. Stalke, *Angew. Chem. Int. Ed.* **2013**, *52*, 1801; *Angew. Chem.* **2013**, *125*, 1845; b) For a discussion of the use of dative bonds in main group compounds see: D. Himmel, I. Krossing, A. Schnepf, *Angew. Chem. Int. Ed.* **2014**, *53*, 370; *Angew. Chem.* **2014**, *126*, 378; c) G. Frenking, *Angew. Chem. Int. Ed.* **2014**, *53*, 6040; *Angew. Chem.* **2014**, *126*, 6152; d) D. Himmel, I. Krossing, A. Schnepf, *Angew. Chem. Int. Ed.* **2014**, *53*, 6047; *Angew. Chem.* **2014**, *126*, 6159.
[25] a) M. Mitoraj, A. Michalak, *Organometallics* **2007**, *26*, 6576; b) M. P. Mitoraj, A. Michalak, T. Ziegler, *J. Chem. Theory Comput.* **2009**, *5*, 962.
[26] a) A. Krapp, K. K. Pandey, G. Frenking, *J. Am. Chem. Soc.* **2007**, *129*, 7596; b) R. Tonner, G. Frenking, *Chem. Eur. J.* **2008**, *14*, 3260.
[27] A. Diefenbach, F. M. Bickelhaupt, G. Frenking, *J. Am. Chem. Soc.* **2000**, *122*, 6449.
[28] R. F. W. Bader, *J. Phys. Chem. A* **2009**, *113*, 10391.
[29] a) H. Braunschweig, R. D. Dewhurst, F. Hupp, M. Nutz, K. Radacki, C. W. Tate, A. Vargas, Y. Ye, *Nature* **2015**, *522*, 327; b) G. Frenking, *Nature* **2015**, *522*, 297.

Received: April 22, 2015
Revised: June 26, 2015
Published online: August 4, 2015

